Asian Journal of Chemistry; Vol. 36, No. 3 (2024), 710-716

ASIAN JOURNAL OF CHEMISTRY

https://doi.org/10.14233/ajchem.2024.31041

Sustainable Synthesis of Porous Biomass-Derived Carbon from *Tecoma capensis* for High Performance Supercapacitors: Characterization and Electrochemical Evaluation

S. THARANI*, and A. PRITHIBA

Department of Chemistry, Avinashilingam Institute for Home Science and Higher Education for Women, Coimbatore-641043, India

*Corresponding author: E-mail: tharaniphd@gmail.com

Received: 10 December 2023; *Accepted*: 6 February 2024; *Published online*: 28 February 2024; AJC-21565

Biowaste carbon products possess interesting physico-chemical properties and are cost-effective due to their remarkable characteristics. Biomass carbon derived from *Tecoma capensis* (TCL) was processed using pyrolysis at a controlled temperature in an eco-friendly, innovative and sustainable way to develop biomass-derived carbon material. The aim of this study is to demonstrate the facile synthesis of porous carbon compounds from biowaste and evaluate their use in supercapacitors. Various analytical methods, such as structural analysis, morphological studies and electrochemical studies, have been employed to characterize the carbon material generated from biomass. Electrochemical performance evaluation was conducted through cyclic voltammetry and galvanostatic charge-discharge studies utilizing 1 M H_2SO_4 and 1 M KOH aqueous electrolyte, which exhibited a specific capacitance of 238 F g^{-1}. The outcomes of the studies suggested that the eco-friendly, straightforward process can be utilized to prepare biomass carbon for the electrochemical energy storage applications in an efficient and sustainable manner.

Keywords: ***Tecoma capensis,*** **Biomass, Pyrolysis, Supercapacitors.**

INTRODUCTION

The release of greenhouse gases from non-renewable conventional fossil fuels is an important factor behind the global demand to switch to renewable energy sources [1-4]. However, some of the most promising sustainable energy options, such as solar, wind and hydropower, are inherently intermittent, necessitating the development of effective energy storage solutions to ensure a stable energy supply [5-7]. Supercapacitors are promising electrochemical energy storage devices that offer distinct advantages, including enhanced safety and extended cycling stability compared to conventional batteries [8-10]. Supercapacitors operate in a dendrite-free and low heat-generation mode, significantly reducing safety concerns [11-13]. Moreover, they boast an impressive cycling life of up to 100,000 cycles, far surpassing that of advanced batteries, which typically endure fewer than 10,000 cycles [11,14]. Supercapacitors show significant potential, especially in conditions that need fast charging and long-term cycle stability. Nevertheless, the energy density of supercapacitors, currently around 5 Wh/kg, falls significantly short of that of batteries, which can reach up to 200 Wh/kg [11,13,15]. The enhancement of the energy density of supercapacitors is a pressing objective.

Carbon materials are extensively employed as electrode materials for supercapacitors and their structure and composition play pivotal roles in enhancing their performance [11]. The supercapacitor capacitance relies on the interfacial reactions occurring on the electrode materials. Carbon materials with high specific surface areas and hierarchical porous structures offer an increased number of reaction sites and superior reaction kinetics [11,16,17]. Additionally, the introduction of heteroatoms through the doping of carbon materials can fine-tune their electronic structure and induce pseudo-capacitance, further enhancing their performance [18].

Biomass-derived carbon is a versatile carbon-based material that is applied across various fields, including catalysts, adsorbents and electrodes [19-22]. Among biomass sources, coconut shells stand out due to their abundant availability, high carbon content, excellent adsorption capabilities and environmental friendliness [23-27]. The conversion of biomass into carbon materials involves carbonization or pyrolysis, where the organic precursors undergo thermal decomposition under controlled

conditions. This results in the formation of carbon materials with tailored properties which are suitable for energy storage applications. Various researchers have investigated the energy-storage properties of biomass-derived carbon materials with and without chemical activation. Sunflower shells [28], marula nutshell waste [29], lotus calyx biowaste [30], hazelnut shell waste [31] and wolfberry fruit biowaste [32] exhibit specific capacitances. *Tecoma capensis*, commonly referred to as cape honeysuckle, is characterized by its distinctive leaves, which hold potential as a biomass waste source for electrode material production. Considering these leaves for the production of electrode materials, their high cellulose content is of particular interest. Cellulose, a complex carbohydrate, can be converted into carbon-rich materials through controlled processes such as pyrolysis or carbonization. This conversion yielded a porous carbon structure with a high surface area, which is advantageous for the electrode applications.

EXPERIMENTAL

The biomass derived from *Tecoma capensis* was procured abundantly from the college campus. Initially, the biomass was subjected to thorough washing and dried in an oven, maintaining a temperature of 60 ºC. For the production of functional carbon, a precisely measured quantity of 10 g of dried leaves powder was subjected to a controlled heating process. This heating was performed in an alumina crucible at an elevated temperature of 700 ºC. Importantly, this thermal transformation occurred in an argon atmosphere, which effectively shielded the material from unwanted interactions. The heating rate was maintained at 10 ºC/min in a tubular furnace. Following a controlled heating process, a solid black residue was obtained and then washed thoroughly with 5 mol/L HCl solution. This step effectively removed any residual impurities and unwanted components from the carbonized material. The material was then dried for 12 h at 60 ºC. The resulting material, derived from the just-carbonized sample at 700 ºC, is denoted as TCL-700 [33].

Characterization: Fourier transform infrared (FT-IR) spectra of the as-prepared TCL were acquired using a Perkin Elmer FT-IR spectrophotometer, employing SOFTWARE-OPUS version 6.5. Spectral analysis covered a frequency range of 4000-400 cm^{-1}. The UV-visible spectra were recorded using a Systronics double-beam spectrometer 2202, spanning a wavelength range of 200-800 nm. X-ray diffraction (XRD) analysis was performed using an X-PERT-PRO Pan analytical diffractometer using Cu*K*α (λ = 1.5406 nm) X-ray source operated at a generator voltage of 45 KV and a current of 30 mA. Raman spectra were obtained utilizing the WiTec alpha 300 instrument, Germany. The surface morphology of activated carbon, in its as-prepared state was examined using a scanning electron microscope (SEM) with a JEOL MODEL JSM 6360 instrument.

Fabrication of electrode: For the electrochemical measurements, biomass-derived carbon (TCL-700) served as the working electrode. TCL-700 carbon, Super-P, in combination with PVDF, was employed as binder at a mass ratio of 85:10:5. The resulting mixture was homogenized to form a paste that was subsequently coated onto the graphene sheet. This three-electrode system featured 1 M KOH and 1 M H_2SO_4 as electrolytes. In this setup, the TCL carbon electrode material was employed as working electrode, Ag/AgCl (SCE) was utilized as reference electrode and platinum was used as counter electrode. Both cyclic voltammetry (CV) and galvanostatic charge-discharge (GCD) analyses were performed within a defined potential range spanning from -0.2 to 0.8 V. Various scan rates ranging from 10 to 50 mV/s were applied during the CV analysis, whereas different current densities at various ranges were considered during the GCD analysis. These electrochemical assessments collectively provide a comprehensive understanding of the electrochemical properties and performance characteristics of TCL-derived carbon materials [34].

RESULTS AND DISCUSSION

Phytochemical screening: A phytochemical screening test was used to identify the active phytochemical constituents present in the leaves extract of *T. capensis* (TCL). The analysis revealed the presence of flavonoids, alkaloids, saponins, steroids and other secondary metabolites in the ethanolic extract of TCL [35,36], which confirmed the presence of several nitrogen- and oxygen-rich compounds. These phytoconstituents in the extract may be responsible for the self-activation of samples with high porosity and conductivity.

FT-IR spectral studies: TCL exhibited distinctive peaks at 3514 cm^{-1} (O-H *str.*), 1516 cm^{-1} (C=C *str.* arom.), 1743 cm^{-1} (C=O *str.*) and 1462 cm^{-1} (C-H bend. in arom.) [37] (Fig. 1a). The FTIR spectrum of TCL-700 revealed distinctive peaks at 2361 cm^{-1} (C≡N *str.*), 1517, 1545 and 1502 cm^{-1} (arom. C=C *str.*) (Fig. 1b), indicating the presence of potentially nitrogen containing and aromatic structures. The peak at 3740 cm^{-1} (O-H *str.*) suggests the existence of hydroxyl groups, which can influence the electrochemical behaviour of the material [38]. Furthermore, the peak at 1742 cm^{-1} (C=O *str.*) indicated the presence of carbonyl groups, while the aliphatic C-H stretching vibrations appeared at 2923 cm^{-1}. The overall composition and structure of TCL-700 material play a crucial role in determining its electrochemical properties.

XRD studies: The XRD spectrum of TCL-700 (Fig. 2) exhibiting the typical peaks around 2θ = 77.5º, 43.9º and 64.5º, which indicates that the prepared TCL carbons represent graphitic carbon [33] or a crystalline nature. The analysis showed that the structure of obtained carbon material was crystalline, as indicated by the miller indices of (222), (220) and (200). Using the Debye-Scherrer's formula, the crystalline size of the carbon material was found to be 31.03 nm [39].

Raman spectral studies: The Raman spectrum of TCL-700 (Fig. 3) and shows the characteristic D and G bands at 1349 and 1583 cm^{-1}, respectively. Typically, the ratio of the intensities of these bands, known as I_D/I_G, serves as an indicator of the degree of graphitization and imperfections within the carbon materials. For TCL-700, the I_D/I_G ratio of 0.98 signifies a prominent level of graphitization, aligned well with the FT-IR spectral analysis.

To precisely determine the positions and widths of the D- and G-bands, a Lorentzian fit was employed. The statistical analysis of the Lorentzian fit yielded an R^2 value of 0.93 for

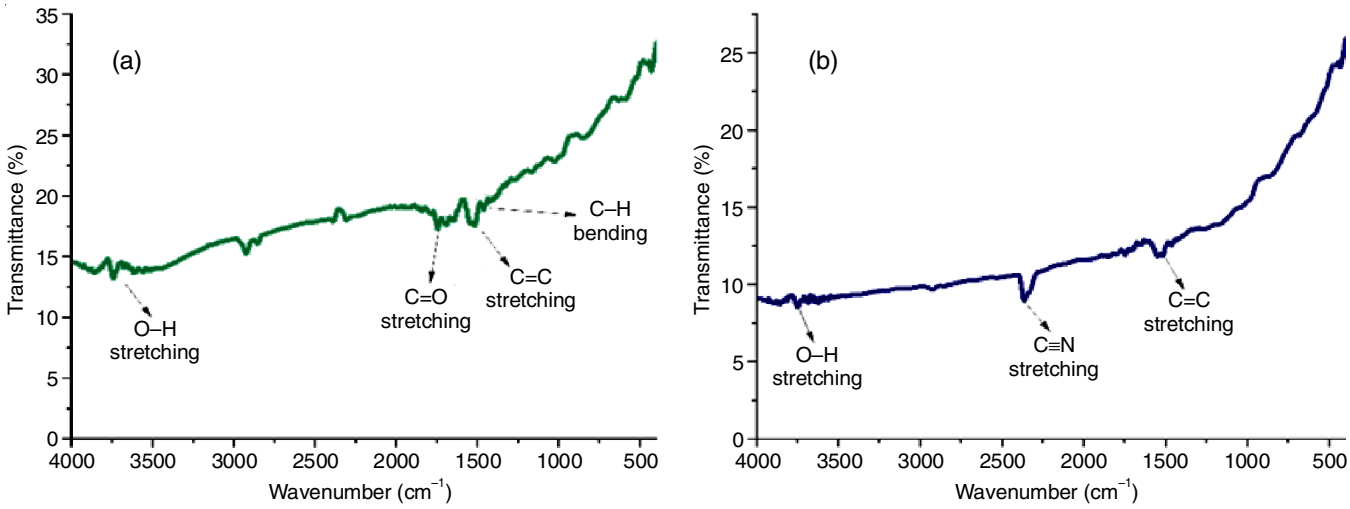

Fig. 1. FTIR spectra of *Tecoma capensis* leaves (a) and TCL-700 (b)

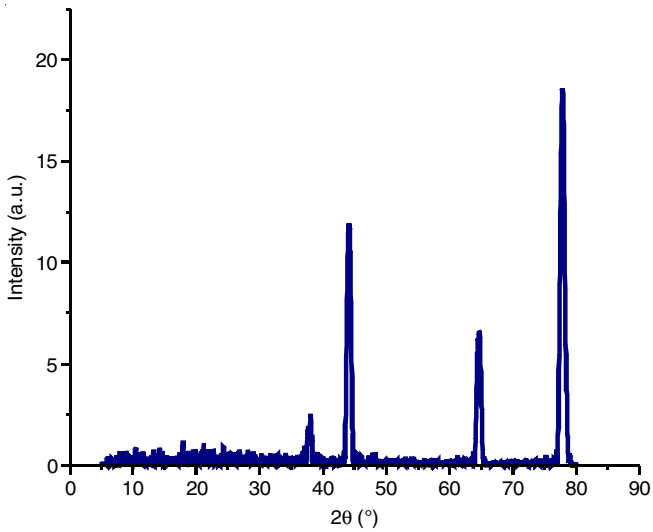

Fig. 2. XRD spectra of TCL-700

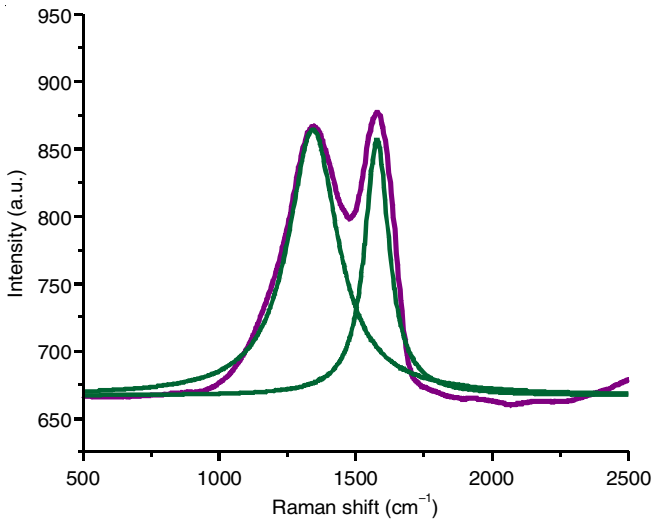

Fig. 3. Raman spectra of TCL-700

TCL-700, indicating an excellent fit of the Lorentzian model to the experimental data. This high R^2 value, near unity, suggests that the regression predictions of the Lorentzian-type model were an exceptional match for the data collected [40-42]. In-plane crystallite size (La) can be determined using the Tuinstra-Koenig relationship:

$$La\ (nm) = (2.4 \times 10^{-10})\ \lambda 4\ (I_D/I_G)^{-1}$$

where $\lambda = 532$ nm which is the Raman excitation wavelength. The values of La are corresponding to the inter defect distance on the surface of the carbon material [41]. The crystalline size of TCL-700 was found to be 17.45 nm.

FE-SEM and EDAX analysis: The FE-SEM images of the TCL produced at 700 ºC are shown in Fig. 4a-e. Additionally, a small number of pores of different sizes may be produced as byproducts of the decomposition and volatilization of raw materials. When the temperature was raised to 700 ºC, large quantities of volatile matter were released at a rapid rate, which caused the particle surface to change, shrink and split during the thermal change. An irregular surface structure was evident in the morphology of TCL-700 material. An increase in the presence of pores and the emergence of elongated channels has been observed in carbon materials [43]. Furthermore, the thermal degradation of chemical bonds and the fusion of certain compounds may result in the rupture of these bonds and alteration of the original material's structure, consequently generating larger pores [44,45].

The elemental composition of the TCL-700 sample was determined by energy-dispersive X-ray analysis (EDAX). The EDAX spectra (Fig. 4f) illustrated the elemental distribution across various regions of the sample surface, revealing the predominant presence of carbon, oxygen and nitrogen atoms in the sample [46].

Thermogravimetric studies: Thermogravimetric analysis (TGA) profiles of the TCL-700 sample are shown in Fig. 5a. These profiles exhibited different stages of weight loss occurring within two distinct temperature ranges *viz.* 85-100 ºC and 650-670 ºC. The former temperature range is attributed to the desorption of physically adsorbed water, whereas the latter corresponds to carbon pyrolysis [47]. Remarkably, even at 1000 ºC, approximately 70% of the initial sample weight remained intact.

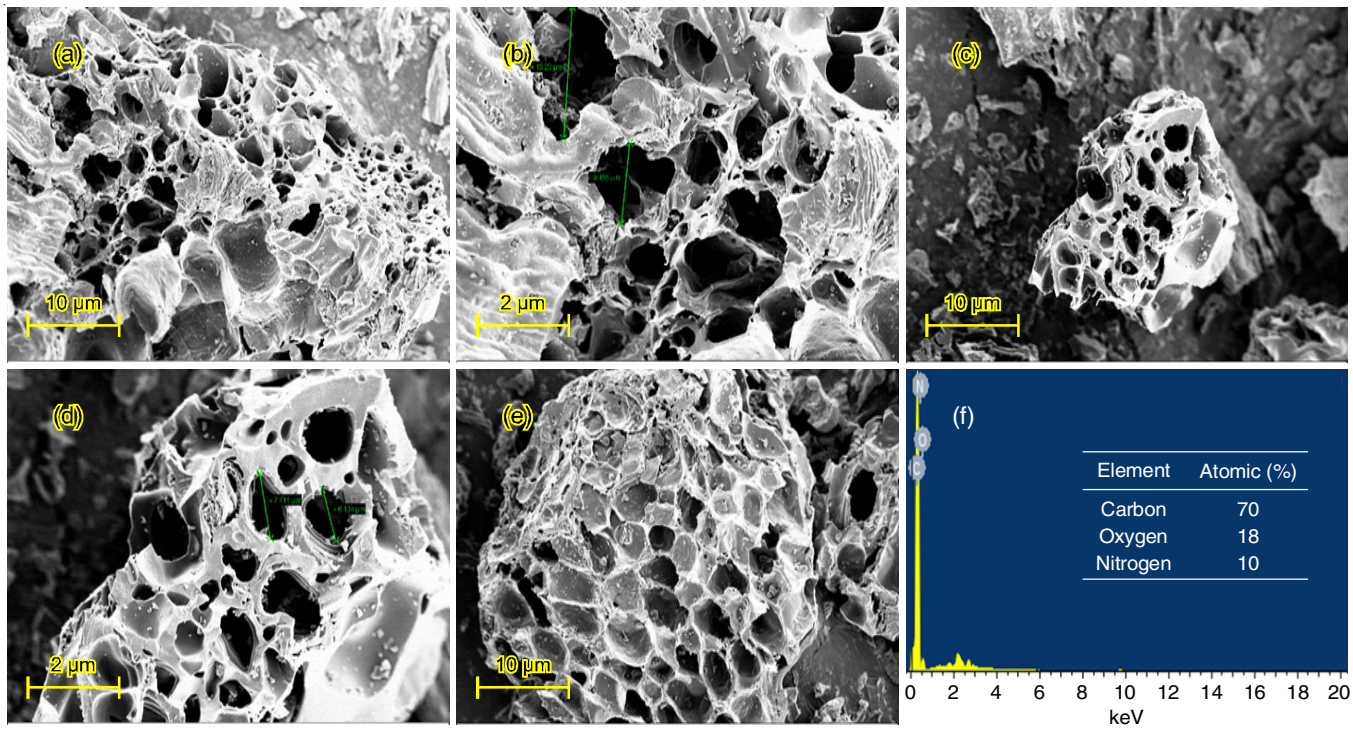

Fig. 4. FE-SEM images and EDAX spectra of TCL-700

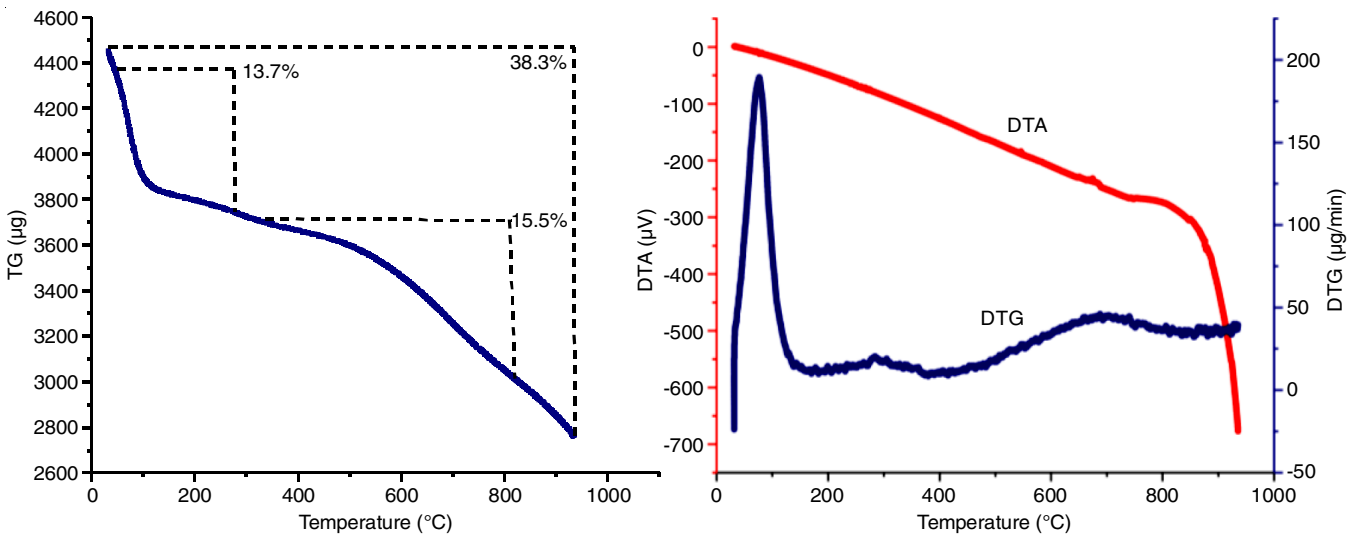

Fig. 5. TG/DTA analysis of TCL-700

Electrochemical measurements: The electrochemical assessment employed a three-electrode system, utilizing the TCL-700 coated electrode as working electrode, Pt as auxiliary electrode and Ag/AgCl as reference electrode, along with 1 M KOH and 1 M H_2SO_4 electrolytes. This setup facilitated galvanostatic charge-discharge (GCD) and cyclic voltammetry (CV) measurements to investigate electrochemical performance. The specific capacitance (Cs) of the carbon electrode material in the three-electrode system was calculated using the discharge characteristics obtained from GCD using the following formula:

$$Cs = I \times \frac{\Delta t}{(\Delta V \times m)}$$

where Cs represents the specific capacitance, I denotes the discharge current, Δt corresponds to the discharge time, m is the mass of the active material and ΔV indicates the potential window after the IR drop [48]. The cyclic voltammetry (CV) measurements of TCL-700 material, conducted using 1 M KOH and 1 M H_2SO_4 solutions as electrolytes and displayed in Fig. 6 within the voltage range of -0.2 to 0.8 V at varying scan rates (10 to 50 mV s^{-1}), provide the valuable insights. An ideal supercapacitor is often characterized by a rectangular cyclic voltammetry (CV) curve. In case of TCL-700 material, an electric double layer capacitor (EDLC) mechanism was evident when using 1 M KOH, while 1 M H_2SO_4 exhibited characteristics of pseudocapacitance. This distinction in behaviour signifies an

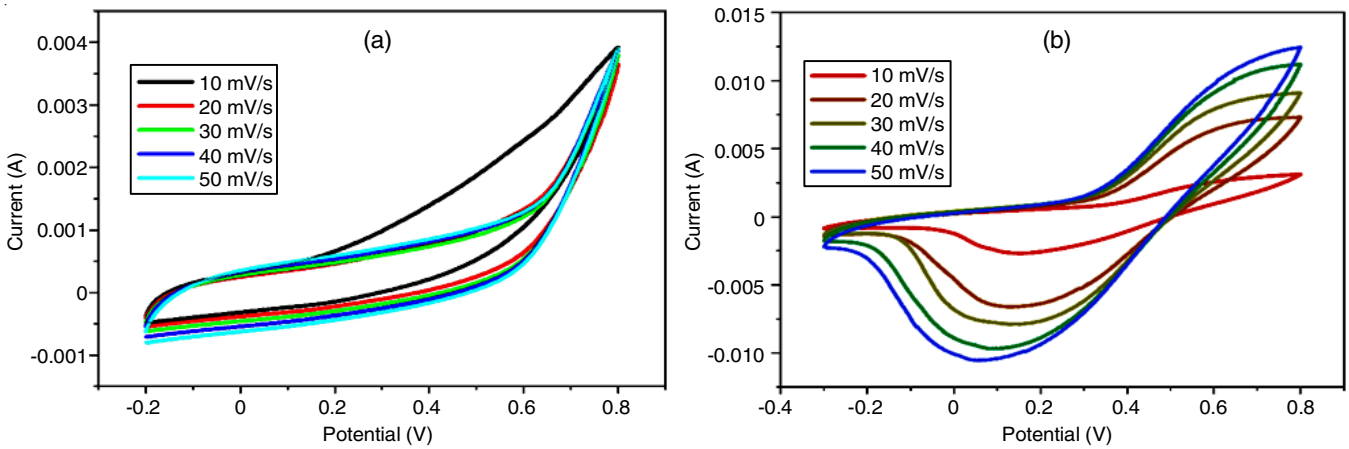

Fig. 6, Cyclic voltammetry of TCL-700 of the electrolyte (a) 1 M KOH and (b) 1 M H_2SO_4

enhancement in the electronic conductivity within the sample. Typically, materials exhibiting pseudocapacitance manifest oxidation and reduction peaks, which were observed in TCL-700, indicating the coexistence of EDLC and pseudocapacitive mechanisms. The presence of chemical bonding in the sample significantly amplified the current levels and facilitated the formation of reduction peaks. In general, the electrochemical stability of EDLC surpasses that of pseudocapacitors, contributing to TCL-700's high electrochemical performance attributed to its exceptional electrochemical properties.

In the galvanostatic charge-discharge (GCD) tests, the existence of mesopores significantly facilitates the swift movement and migration of ions during the charging/discharging phases. The GCD curves of TCL-700, illustrated in Fig. 7 across a potential range of -0.4 V to 0.4 V at various current densities ranging from 75 to 250 μA g^{-1}, revealed specific capacitance values of 238 F g^{-1} and 32.42 F g^{-1} for 1 M KOH and 1 M H_2SO_4, respectively. TCL-700 material displayed nearly triangular GCD profiles indicating the electric double-layer capacitor (EDLC) behaviour primarily with a minor pseudocapacitive effect.

Furthermore, the impedance spectra of TCL-700 presented in Fig. 8 showed the equivalent series resistance (ESR) intercepting the real axis in the high-frequency zone within electrochemical impedance spectroscopy (EIS). The ESR measurements exhibited a significant decrease in the presence of 1 M H_2SO_4 (9.8 Ω) as compared to 1 M KOH (14.8 Ω), suggesting a higher level of conductivity in the former (Table-1). Similarly, the charge transfer resistance values of 10.4 Ω and 13.8 Ω were observed for 1 M KOH and 1 M H_2SO_4, respectively. The elevated charge transfer resistance in 1 M H_2SO_4 is attributed to the combination of poor electrode conductivity and electrolyte characteristics. These findings provide insight into the electrochemical characteristics of TCL-700 material, confirming its capacity for efficient energy storage and utilization [49].

Conclusion

In conclusion, the utilization of *Tecoma capensis* (TCL) biowaste through controlled-temperature pyrolysis has proven to be a promising and eco-friendly approach to produce biomass derived carbon with the exceptional properties. Comprehensive characterization involving the structural, morphological and electrochemical analyses revealed the potential of this carbon material for the supercapacitor applications. The synthesized biomass carbon material exhibited a specific capacitance of 230 F g^{-1} in both 1 M H_2SO_4 and 1 M KOH electrolytes indicating its viability for energy storage. These findings not only emph-

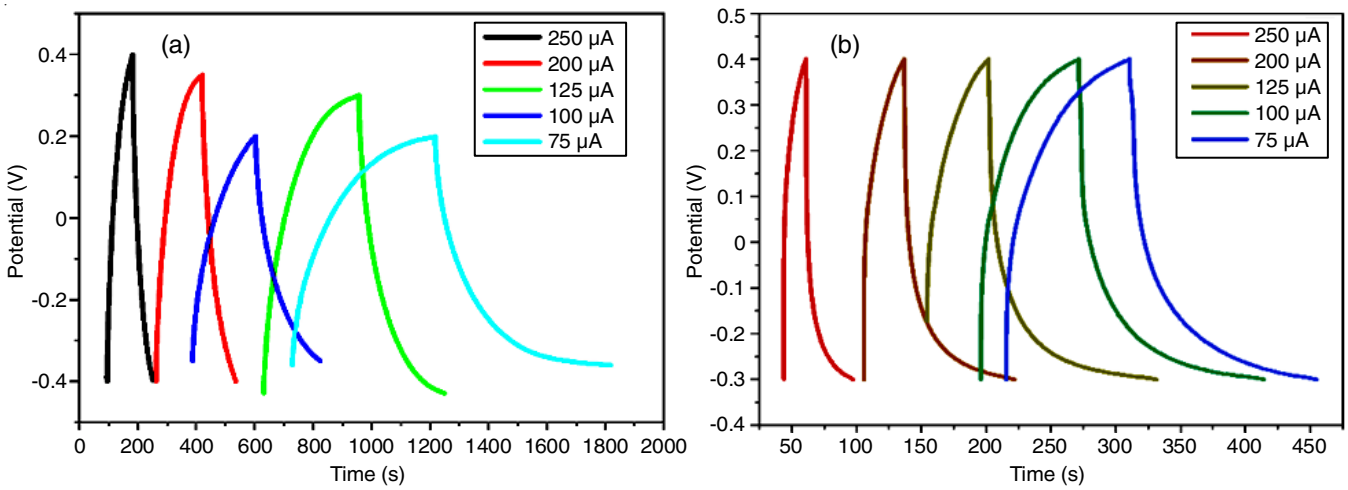

Fig. 7. GCD measurements of TCL-700 of the electrolyte (a) 1 M KOH and (b) 1 M H_2SO_4

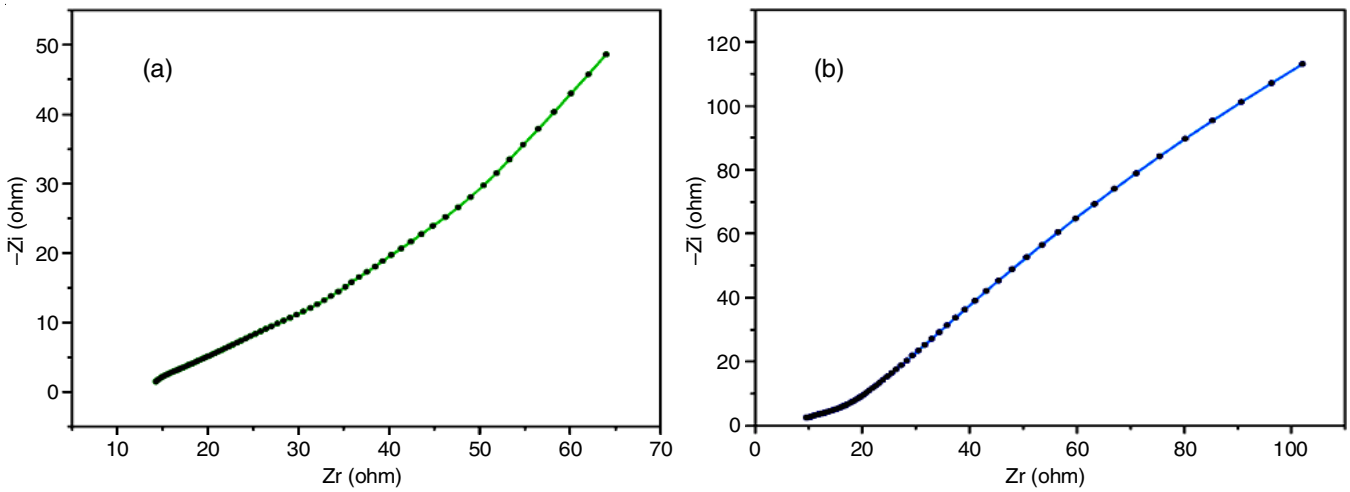

Fig. 8. Electrochemical impedance spectra of TCL-700 of the electrolyte (a) 1 M KOH and (b) 1 M H_2SO_4

TABLE-1
ELECTROCHEMICAL MEASUREMENTS OF TCL-700

Current density (μA)	Capacitance (F/g)		Scan rate (mV/s)		Capacitance (F/g)	
	KOH	H_2SO_4	KOH	H_2SO_4	KOH	H_2SO_4
250	54.4	21.63	10	10	112	186.5
200	73.6	28.46	20	20	38.4	228.7
125	238.8	32.42	30	30	27.4	188.9
100	68.48	28.46	40	40	23.6	171.9
75	238.8	21.63	50	50	20.9	148.7

asize the ease of synthesizing porous carbon from biowaste but also highlight its significant electrochemical performance, positioning it as a suitable candidate for scalable applications in electrochemical energy storage systems.

CONFLICT OF INTEREST

The authors declare that there is no conflict of interests regarding the publication of this article.

REFERENCES

1. S. Zhong, H. Zhu, L. Yang, X. Chi, W. Tan and W. Weng, *J. Mater. Chem. A Mater. Energy Sustain.*, **11**, 8101 (2023); https://doi.org/10.1039/D3TA00367A
2. J. Zhou, H. Xiao, W. Weng, D. Gu and W. Xiao, *J. Energy Chem.*, **50**, 280 (2020); https://doi.org/10.1016/j.jechem.2020.03.048
3. X. Chen, H. Zhao, J. Qu, D. Tang, Z. Zhao, H. Xie, D. Wang and H. Yin, *Green Chem.*, **22**, 7946 (2020); https://doi.org/10.1039/D0GC02626C
4. W. Weng, B. Jiang, Z. Wang and W. Xiao, *Sci. Adv.*, **6**, 9278 (2020); https://doi.org/10.1126/sciadv.aay9278
5. Y. Gogotsi, *ACS Nano*, **8**, 5369 (2014); https://doi.org/10.1021/nn503164x
6. G. Kothandam, G. Singh, X. Guan, J.M. Lee, K. Ramadass, S. Joseph, M. Benzigar, A. Karakoti, J. Yi, P. Kumar and A. Vinu, *Adv. Sci.*, **10**, 2301045 (2023); https://doi.org/10.1002/advs.202301045
7. W. Weng, S. Wang, W. Xiao and X.W.D. Lou, *Adv. Mater.*, **32**, 2001560 (2020); https://doi.org/10.1002/adma.202001560
8. T. Jiang, Y. Wang and G.Z. Chen, *Small Methods*, **7**, 2201724 (2023); https://doi.org/10.1002/smtd.202201724
9. A.T. Prasannakumar, R.R. Mohan, R. Rohith, V. Manju and S.J. Varma, *ChemistrySelect*, **8**, 202203564 (2023); https://doi.org/10.1002/slct.202203564
10. J. Hao, L. Yan, X. Zou, Y. Bai, Y. Han, C. Zhu, Y. Zhou and B. Xiang, *Small*, **19**, 2300467 (2023); https://doi.org/10.1002/smll.202300467
11. P. Simon, Y. Gogotsi and B. Dunn, *Science*, **343**, 1210 (2014); https://doi.org/10.1126/science.1249625
12. Z. Qiu, Z. Liu, X. Lu, S. Zhang, Y. Yan, C. Chi, C. Huangfu, G. Wang, P. Gao, W. Chi, Z. Xu, T. Wei and Z. Fan, *Small*, **19**, 2302316 (2023); https://doi.org/10.1002/smll.202302316
13. Y. Guan, Y. Cong, R. Zhao, K. Li, X. Li, H. Zhu, Q. Zhang, Z. Dong and N. Yang, *Small*, **19**, 2301276 (2023); https://doi.org/10.1002/smll.202301276
14. Q. Zhang, Y. He, G. Lin, X. Ma, Z. Xiao, D. Shi and Y. Yang, *J. Mater. Chem. A Mater. Energy Sustain.*, **9**, 10652 (2021); https://doi.org/10.1039/D1TA00302J
15. X. Li, W. Li, Q. Liu, S. Chen, L. Wang, F. Gao, G. Shao, Y. Tian, Z. Lin and W. Yang, *Adv. Funct. Mater.*, **31**, 2008901 (2021); https://doi.org/10.1002/adfm.202008901
16. J. Cao, J. Luo, P. Wang, X. Wang and W. Weng, *Mater. Technol.*, **35**, 522 (2020); https://doi.org/10.1080/10667857.2019.1699270
17. Y. Cheng, L. Wu, C. Fang, T. Li, J. Chen, M. Yang and Q. Zhang, *J. Mater. Res. Technol.*, **9**, 3261 (2020); https://doi.org/10.1016/j.jmrt.2020.01.022
18. C. Zhang, X. Liu, Z. Li, C. Zhang, Z. Chen, D. Pan and M. Wu, *Adv. Funct. Mater.*, **31**, 2101470 (2021); https://doi.org/10.1002/adfm.202101470
19. D. Cao, Q. Li, X. Sun, Y. Wang, X. Zhao, E. Cakmak, W. Liang, A. Anderson, S. Ozcan and H. Zhu, *Adv. Mater.*, **33**, 2105505 (2021); https://doi.org/10.1002/adma.202105505
20. Q. Li, D. Cao, M.T. Naik, Y. Pu, X. Sun, P. Luan, A.J. Ragauskas, T. Ji, Y. Zhao, F. Chen, Y. Zheng and H. Zhu, *ACS Sustain. Chem. Eng.*, **10**, 8704 (2022); https://doi.org/10.1021/acssuschemeng.2c00783

21. Q. Li, X. Sun, D. Cao, Y. Wang, P. Luan and H. Zhu, *Electrochem. Energy Rev.*, **5**, 18 (2022); https://doi.org/10.1007/s41918-022-00170-6
22. X. Sun, Q. Li, D. Cao, Y. Wang, A. Anderson and H. Zhu, *Small*, **18**, 2105678 (2022); https://doi.org/10.1002/smll.202105678
23. S.R.A. Sasono, M.F. Rois, W. Widiyastuti, T. Nurtono and H. Setyawan, *Results Eng.*, **18**, 101070 (2023); https://doi.org/10.1016/j.rineng.2023.101070
24. S.M. Omokafe, A.A. Adeniyi, E.O. Igbafen, S.R. Oke and P.A. Olubambi, *Int. J. Electrochem. Sci.*, **15**, 10854 (2020); https://doi.org/10.20964/2020.11.10
25. K.C. Lee, M.S.W. Lim, Z.Y. Hong, S. Chong, T.J. Tiong, G.T. Pan and C.M. Huang, *Energies*, **14**, 4546 (2021); https://doi.org/10.3390/en14154546
26. M.F.M. Yusop, E.M.J. Jaya, A.T. Mohd Din, O.S. Bello and M.A. Ahmad, *Chem. Eng. Technol.*, **45**, 1943 (2022); https://doi.org/10.1002/ceat.202200051
27. Z. Yang, G. Yan, X. Liu, Z. Feng, X. Zhu, Y. Mao, S. Chen, Z. Yu, R. Fan and L. Shan, *J. Renew. Mater.*, **10**, 3573 (2022); https://doi.org/10.32604/jrm.2022.022031
28. Y. Tan, Y. Ren, Z. Xu, Y. Zhu and H. Li, *J. Electron. Mater.*, **52**, 2603 (2023); https://doi.org/10.1007/s11664-023-10223-1
29. B. Shaku, T.P. Mofokeng, N.J. Coville, K.I. Ozoemena and M.S. Maubane-Nkadimeng, *Electrochim. Acta*, **442**, 141828 (2023); https://doi.org/10.1016/j.electacta.2023.141828
30. G. Dhakal, D. Mohapatra, Y.I. Kim, J. Lee, W.K. Kim and J.J. Shim, *Renew. Energy*, **189**, 587 (2022); https://doi.org/10.1016/j.renene.2022.01.105
31. P. Ozpinar, C. Dogan, H. Demiral, U. Morali, S. Erol, C. Samdan, D. Yildiz and I. Demiral, *Renew. Energy*, **189**, 535 (2022); https://doi.org/10.1016/j.renene.2022.02.126
32. X. Xu, K. Sielicki, J. Min, J. Li, C. Hao, X. Wen, X. Chen and E. Mijowska, *Renew. Energy*, **185**, 187 (2022); https://doi.org/10.1016/j.renene.2021.12.040
33. M. Biswal, A. Banerjee, M. Deo and S. Ogale, *Energy Environ. Sci.*, **6**, 1249 (2013); https://doi.org/10.1039/c3ee22325f
34. G. Byatarayappa, V. Guna, R.M. G, K. Venkatesh, Y. Zhao, N. N, N. Reddy and K. Nagaraju, *Sustain. Energy Fuels*, **6**, 4034 (2022); https://doi.org/10.1039/D2SE00802E
35. I. Kavya, D.S. Kumar, D. Sandhya, P. Janaki and M.C. Eswaraiah, *Indian J. Res. Pharm. Biotechnol.*, **3**, 410 (2015).
36. S.N. Kumar and N. Thampi, *J. Chem. Pharm. Res.*, **7**, 840 (2015).
37. N. Sudhan, K. Subramani, M. Karnan, N. Ilayaraja and M. Sathish, *Energy Fuels*, **31**, 977 (2017); https://doi.org/10.1021/acs.energyfuels.6b01829
38. X. Ma, H. Wang, Q. Wu, J. Zhang, D. Liang, S. Lu and Y. Xiang, *J. Electrochem. Soc.*, **166**, A236 (2019); https://doi.org/10.1149/2.0831902jes
39. N. Katagiri, N. Adachi and T. Ota, *J. Ceram. Soc. Jpn.*, **122**, 29 (2014); https://doi.org/10.2109/jcersj2.122.29
40. D. Wang, Y. Min and Y. Yu, *J. Solid State Electrochem.*, **19**, 577 (2015); https://doi.org/10.1007/s10008-014-2639-0
41. F. Giannazzo, R. Dagher, E. Schilirò, S.E. Panasci, F. Roccaforte, G. Greco, G. Nicotra,S. Agnello, J. Brault, Y. Cordier and A. Michon, *Nanotechnology*, **32**, 015705 (2021); https://doi.org/10.1088/1361-6528/abb72b
42. P. Divya and R. Rajalakshmi, *Mater. Today Proc.*, **27**, 44 (2020); https://doi.org/10.1016/j.matpr.2019.08.200
43. C. Pituello, O. Francioso, G. Simonetti, A. Pisi, A. Torreggiani, A. Berti and F. Morari, *J. Soils Sediments*, **15**, 792 (2015); https://doi.org/10.1007/s11368-014-0964-7
44. P. Fu, S. Hu, J. Xinag, L. Sun, T. Yang, A. Zhang, Yi Wang and G. Chen, 2009 International Conference on Energy and Environment Technology, Guilin, China, pp. 109-112 (2009); https://doi.org/10.1109/ICEET.2009.33
45. S. Suman and S. Gautam, *Energy Sources A Recovery Util. Environ. Effects*, **39**, 761 (2017); https://doi.org/10.1080/15567036.2016.1263252
46. S. Suman, D.S. Panwar and S. Gautam, *Energy Sources A Recovery Util. Environ. Effects*, **39**, 1007 (2017); https://doi.org/10.1080/15567036.2017.1283553
47. S. Tharani, *ECS Trans.*, **107**, 14433 (2022); https://doi.org/10.1149/10701.14433ecst
48. A. Khan, R. Arumugam Senthil, J. Pan, Y. Sun and X. Liu, *Batter. Supercaps*, **3**, 731 (2020); https://doi.org/10.1002/batt.202000046
49. S. Palanisamy, S.K. Kandasamy, S. Thangmuthu, D.K. Selvarasu, M. Panchanathan, P.V. Ramanai and B.S. Gevert, *J. Mater. Sci. Mater. Electron.*, **32**, 25175 (2021); https://doi.org/10.1007/s10854-021-06974-4